Study of the Vacuum Degassing Process Using the Effective Equilibrium Reaction Zone Model

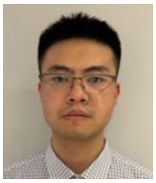

Advanced steel products made by electric arc furnace steelmaking require vacuum degassing (VD) to meet nitrogen/hydrogen specifications. An effective equilibrium reaction zone-based VD model was developed to understand/optimize the operational parameters and their impact on denitrogenation (deN) rate. The effects of argon injection, vacuum pressure and steel temperature were explored. The calculated deN rates were validated with industrial-scale tank degasser trials. A novel approach was adopted to incorporate bubble-steel interface deN reactions in order to replicate plume and eye formation through Ar injection in VD.

Authors

Bikram Konar (left), Senior Research Engineer, Research and Development, EVRAZ North America, Regina, Sask., Canada
bikram.konar@evrazna.com

Keyan Miao (right), Process Engineering Specialist, Stelco Inc., Nanticoke, Ont., Canada; formerly with Research and Development, EVRAZ North America, Regina, Sask., Canada

Noah Quintana, EVRAZ North America, Pueblo, Colo., USA

Ziyi Wang, EVRAZ North America, Regina, Sask., Canada

Introduction

Vacuum degassing (VD) plays a pivotal role within modern electric arc furnace (EAF)-based steelmaking operations, enhancing the quality and purity of molten steel by addressing the removal of undesirable gaseous elements (predominantly nitrogen and hydrogen). VD contributes to denitrogenation,[1–4,7] dehydrogenation,[4,5] desulfurization,[4,6,7] decarburization,[4,7] and inclusion removal.[8,9] The primary objective of VD is to achieve the required amount of N and H in the steel, leading to improved consistency in mechanical properties and better reliability in downstream thermomechanical processing.

The removal of gases during VD involves several key mechanisms:

1. Bubble absorption: Nitrogen and other gases dissolved in the liquid steel are absorbed by rising inert gas bubbles, such as argon, introduced into the molten metal.
2. Open-eye region direct denitrogenation: As rising gas bubbles displace the slag cover on the molten steel's top surface, an open-eye region is created. This exposes the liquid steel to low vessel pressures which facilitates the escape of gases directly into the ambient atmosphere.
3. Spontaneous bubble generation: Gaseous elements may also form spontaneous bubbles within the steel bath, contributing to the overall degassing process.

During VD processing, operators tend to follow similar profiles for Ar injection along with the pressure regulation of the degassing vessel. With variation of incoming steel chemistry (N, S, O and other elements), modification of set profiles is necessitated by the operator. The lack of guidance for the operators amidst concerns of steelmaking delays often leads to suboptimal operation. This situation can often be compounded by maintenance issues and malfunctions at the VD station. Thus, a predictive model for VD operation considering operational parameters (Ar, pressure regulation profiles) and steel chemistry will be highly effective to improve process efficiency.

In this work, a vacuum tank degasser (VTD) model is proposed to simulate the denitrogenation (deN) process using the effective equilibrium reaction zone (EERZ) approach.[10,11] The EERZ-based model facilitates the partitioning of complicated metallurgical processes into distinct and simplified reaction zones, each assumed to be in thermodynamic equilibrium for a modeled time scale zone homogenization frequency. The replication of kinetics within the EERZ model involves adjusting reaction zone volumes and homogenization frequencies. These volumes depend on specific reaction mechanisms, prevailing process conditions and the rate of phase mixing. Estimations of reaction zone volumes can be derived from various sources, such as physical modeling performed using water models, other phenomenological models, and plant observations and measurements. In this work, primarily nitrogen removal is simulated. The resulting model is then used to derive a simple correlation which can predict N content of the steel as a function of Ar, pressure profile, initial N and S content. This approach offers a synergistic blend of modeling the thermodynamic and kinetic aspects of the VD process and utilizing plant data/observations to better understand and optimize VD efficiency in steelmaking operation.

Plant Operation and Analysis

General Operation

EVRAZ North America's Pueblo, Colo., USA, operation is primarily scrap-based, which produces steel using a single EAF. The steel is then refined at the ladle furnace (LF), followed by the vacuum tank degasser (VTD), and subsequently cast into rounds with diameters ranging from 7.5 inches to 12.25 inches in a 6-strand continuous caster. The VTD at the Pueblo operation utilizes a single porous plug for argon injection. During VD, the automation system records the amount of argon injected (in SCF), vessel pressure (in torr), and the VTD is equipped with an air-cooled high-definition camera and vibration sensors.

Fig. 1 illustrates a schematic of an ideal VD processing, where ambient pressure is decreased, and Ar gas injection is increased to their respective minimum and maximum values during the deep-vacuum stage. As the VD process enters this stage, the slag eye becomes visible. Video feed from the camera and data from vibration sensors are continuously recorded throughout the VD process. In this work, the observed slag eye images are discussed in the following section and have been used as a key tool to constrain one of the parameters of the EERZ model. While on-line offgas monitoring could have provided a more holistic understanding of the process thermodynamics and kinetics, it was not conducted during the heats discussed in this study. Both slag/steel samples were acquired at t_{start} and t_{finish} at 1 atm (without vacuum). The difference of t_{start} and t_{finish} can be considered as the actual time (seconds). Utilizing on-line feedback and steel/slag sampling with offgas monitoring will be sufficient to derive a computational model of the VD process and predict its kinetics.

Process Data: Ar Injection Data/Vacuum Visualization

Pueblo's VTD automation records real-time measurements of argon flow and pressure at the porous plug, along with the vessel pressure (ambient atmosphere to which the ladle is exposed). During the degassing process, an air-cooled high-definition camera captures the top surface of the ladle, recording the slag cover and the steel eye/spout when exposed to the atmosphere. The video recorded by the camera can be correlated with other real-time process parameters.

Fig. 2 illustrates a typical VD processing sequence, showcasing recorded ambient atmosphere pressure, Ar gas injection rates and snapshots from a standard video camera feed at specific instances during the processing time. The observations made at these instances are as follows:

a. Approximately 300 seconds: The vessel pressure is sufficiently low (<0.1 bar), and the ladle eye starts becoming visible. However, at this point, the ladle eye is still unstable (wobbly) and may close and reopen. The lower vessel pressure also aids in reducing dust, ultimately improving the clarity of the video feed.

b. Approximately 550 seconds: VD enters the deep-vacuum stage (<0.01 bar), leading to the stabilization of the ladle eye.

c. Approximately 650 seconds: VD continues in the deep-vacuum stage, and with the increase in the argon injection rate, the ladle eye size experiences a significant increase.

Figure 1

Schematic of a typical vacuum tank degassing process, including primary process parameters, real-time process data and materials during the operation.

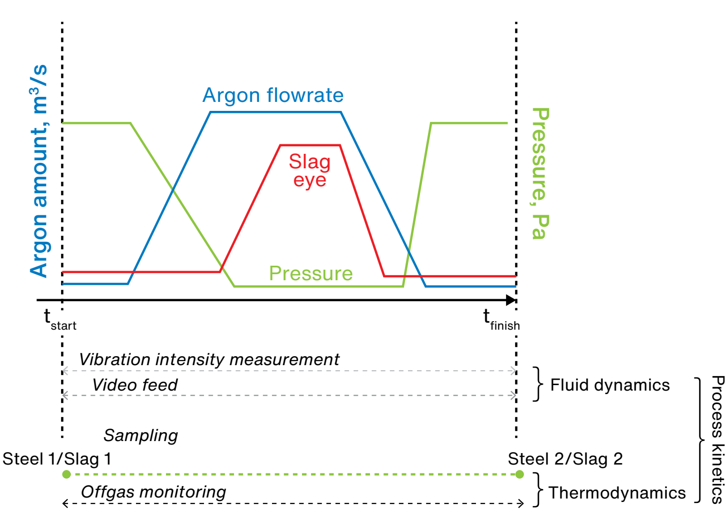

Figure 2

Snapshots from the video recording at different processing instances: 300 seconds (a), 550 seconds (b), 650 seconds (c) and 800 seconds (d) along with the vessel pressure and Ar injection rate.

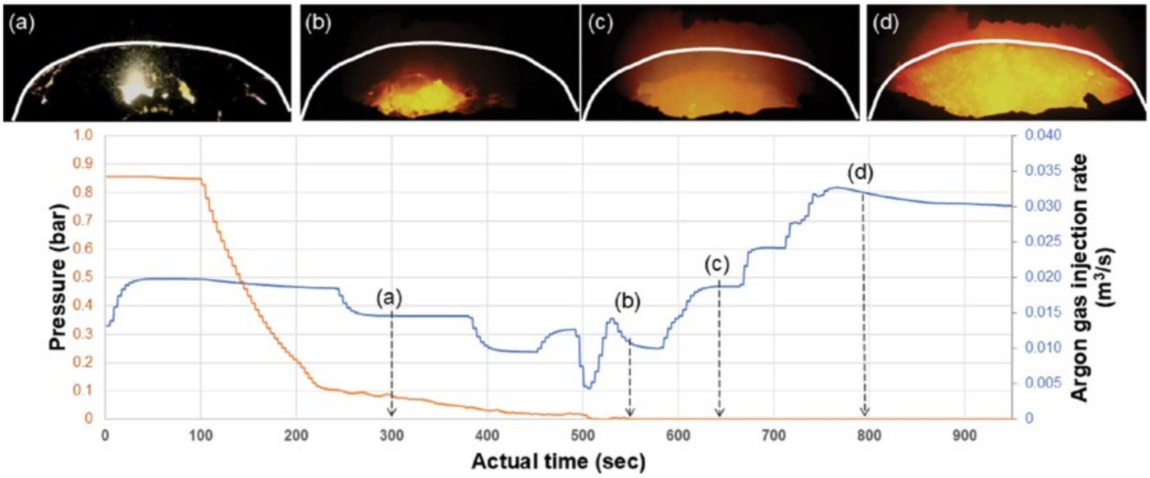

d. Approximately 800 seconds: VD, with the maximum argon injection rate and low vessel (deep vacuum) pressure, results in a significantly turbulent ladle eye with bubbly steel and occasional splashes. The ladle eye size extends to almost 80% of the ladle diameter, and there is notable mixing between hot steel and slag layers.

The video stream is continuously monitored on-line to verify the performance of the Ar plug. In the present work, the video and time-specific snapshot data have been further analyzed, incorporating image processing techniques for measuring the ladle eye size. Based on these observations the VD process model is performed for processing time (seconds): [actual time 250] seconds.

Production Sampling and Analysis and Automation

The chemical compositions of VTD slag and steel samples are analyzed as follows:

a. Steel samples: Elemental constituents are measured using an optical emission spectrometer (OES, ARL Model 4460). Steel lollipops extracted from the heats are employed for this analysis.

b. Slag samples: Elemental constituents are determined using an x-ray fluorescence (XRF) analyzer (Bruker S8 Tiger). The XRF analysis involves a finely ground powder of the slag sample and identifies slag components based on internal calibration.

In this, three heats were employed to model and validate the VD process using the EERZ approach. Tables 1 and 2 present summaries of the steel and slag chemistries of the three heats before the VD process. The measurements of steel chemistry before and after the VD process

Table 1

Steel Chemistry Entering the Vacuum Tank Degasser

Heats	Fe, wt. %	C, wt. %	Mn, wt. %	Si, wt. %	S, ppm	N, ppm
1	~98.5	0.76	0.76	0.245	130	93
2	~98.5	0.55	0.71	0.265	130	77
3	~98.5	0.22	0.60	0.200	120	62

Table 2

Slag Chemistry Entering the Vacuum Tank Degasser

Heats	CaO	Al_2O_3	SiO_2	MgO	FeO	MnO
1	49.1	7.0	33.0	9.7	0.9	0.3
2	47.8	5.0	31.9	13.4	1.4	0.6
3	53.9	3.2	29.7	12.0	1.0	0.2

were crucial for modeling and interpreting the results within the EERZ framework. In the current iteration of the VD process model, the slag chemistry data were primarily used in density calculation equations to determine the ladle eye size.

Modeling Implementation and Workflow

Effective Equilibrium Reaction Zone Modeling

The EERZ model has been employed to model the VD process. Recently, various steelmaking processes[10,11] have been successfully modeled using the EERZ framework, leveraging FactSage[12] thermodynamic databases. EERZ modeling enables the decoupling of complex metallurgical processes into a finite number of reaction zones. An effective reaction zone (ERZ) is a modeled volume comprising multiple phases and a reaction interface that is assumed to reach equilibrium. To maintain the process continuum, adjacent reaction zones homogenize at another modeled frequency. Consequently, the kinetics of a process are simulated by modifying the effective reaction zone volumes and homogenization frequency. The accuracy of EERZ modeling relies on experimental/industrial process data, plant measurements/observations, and computational fluid dynamic/physical modeling of the process. In the present work, all reactions are considered isothermal/adiabatic, as the vacuum tank degassing process does not involve any active combustion reaction. The determination of the homogenization frequency, guided by the momentum or fluid dynamic aspects of adjacent zones, governs how often these zones equilibrate.

Fig. 3 provides a schematic representation of a VTD segmented into its ERZs, illustrating different reactions, including gas bubbles. The deN reaction modes are:

Nitrogen and other gases dissolved in the liquid steel are absorbed by rising inert gas bubbles, such as argon, introduced into the molten metal.

$$[N]_{bulk}+[N]_{bulk}+(Ar)_{bubble}\rightarrow(Ar+N_2)_{bubble}$$

(Eq. 1)

Argon bubbles rise in the plume and become enriched with nitrogen and/or other dissolved gases.

$$[N]_{bulk}+[N]_{bulk}+(Ar+N_2)_{bubble}\rightarrow(Ar+2N_2)_{bubble}$$

(Eq. 2)

Spontaneous gas bubbles of nitrogen form at the ladle's open eye, where the steel is directly exposed to the vacuum conditions under which the VTD is operating.

$$[N]_{bulk}+[N]_{bulk}\rightarrow(N_2)_{Vacuum}$$

(Eq. 3)

Spontaneous nitrogen gas bubble formation in the bulk steel volume.

$$[N]_{bulk}+[N]_{bulk}\rightarrow(N_2)_{bubble}$$

(Eq. 4)

These modes will be referred to in the section titled EERZ Modeling Parameters, Tools and Databases while explaining the VTD modeling flow sheet.

In the current vacuum tank degassing simulation, there are three ERZs:

a. Zone at Eye (Z_eye): The volume of steel at the ladle eye (or sprout region) that is exposed to the ambient atmosphere when the slag cover breaks due to the plume is classified as Z_eye. The ambient atmosphere is adjusted based on the vessel pressure data obtained from the VTD operation. In this study, the dimensionless eye (A_e/A_p) was calculated using relations derived by Krishnapisharody and Irons:[13,14]

Figure 3

Schematic diagram of the vacuum tank degasser and the reaction zones included in the Effective Equilibrium Reaction Zone (EERZ)-based model. Black arrows indicate steel flow, while violet lines within the plume represent different reaction zones considered in the Z1 calculations. The dotted plume outlines volume changes at varying Ar injection rates. The four modes [1–4] of the deN reaction are illustrated in the insets.

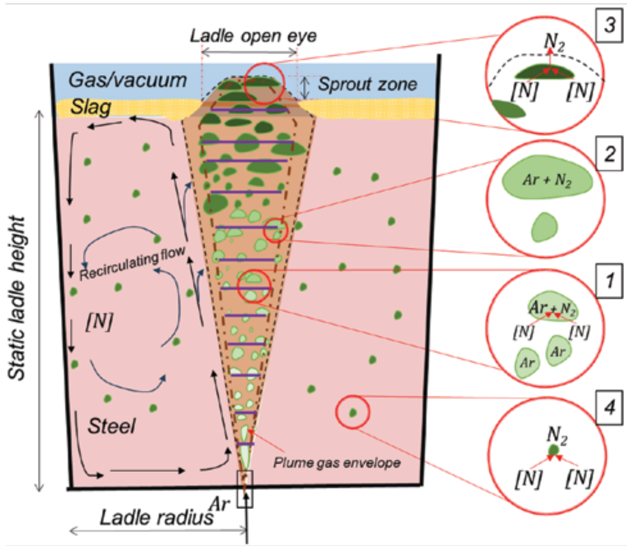

$$\frac{A_e}{A_p} = \begin{cases} 0.91 - 0.12\chi^{-2}, \chi < 0.6 \\ 0.185 - 0.06\chi^{-2} + 2.535\chi, 0.6 \le \chi < 0.75 \\ -0.54 + 5.07\chi, \chi \le 0.75 \end{cases}$$

(Eq. 5)

where χ is dependent on the slag (ρ_s) and steel (ρ_l) densities, Ar gas flowrate ($\dot{Q}_l$), standard condition gas flowrate ($\dot{Q}_N$), liquid steel height (H) and slag height (h_s). χ is calculated as:

$$\chi = \left(1 - \frac{\rho_s}{\rho_l}\right)^{-0.5} \left(\frac{\dot{Q}_l}{g^{0.5} H^{2.5}}\right)^{0.32} \left(\frac{h_s}{H}\right)^{-0.5}$$

(Eq. 6)

and the plume area is given by:[14]

$$A_p = 1.41\left(Q^*\right)^{0.4} H^2$$

(Eq. 7)

Slag density was estimated to be around 2,800 kg/m^3 (based on the respective slag chemistries), and slag height was measured to be 0.1 m (using pipe dips in the ladle station). During the process, Ar gas flowrate varies; therefore, a Microsoft Excel-based Plume Eye Solver was developed using Eqs. 5–7 to calculate A_e/A_p and ladle eye size. Fig. 4 illustrates the schematic representation of A_e/A_p and its variation as a function of the volumetric Ar flowrate as calculated by Plume Eye Solver.

Fig. 5 shows a snapshot from the video recording of the ladle eye/sprout zone during the degassing operation and the comparison between the measured and calculated ladle eye diameter over the processing time of 1,000 seconds (~20 minutes). As can be seen in Fig. 5b, ladle eye diameter measurements were reproduced by that calculated by Plume eye solver. The differences between the calculation and measurements can be attributed to high-temperature steel/slag/Ar fluid flow uncertainties and errors introduced in the measurements by exposure, strong bubbling, movement of the liquid steel and a one-dimensional observation of the sprout.

b. Zone 1 (Z1) — Gas-Steel Interface: As shown in Fig. 6, Z1 represents an interface zone between the gas bubbles and the steel in the plume (Zone 2 is explained in the following section). As illustrated in Fig. 6a, deN reaction is simulated by considering the amount of steel around the bubble, constituting Z1. The nitrogen in the plume (N_Z2) serves as a buffer where the nitrogen in the Z1 steel (N_Z1) reacts (reaction: R1) with the Ar (and N_2) in the bubbles during active denitrogenation. To capture the evolution of gases and sizes of the bubbles, the Ar plume generated in the VTD is segmented into "n" sections (14 for the optimized EERZ presented here). Each respective section experiences different ferrostatic pressure heads and flow conditions (argon gas injection rate) during the vacuum degassing (VD) process. The bubble size, therefore, changes depending on the local volumetric steel flowrate. Consequently, Z1 at a given segment (Z1_n) and across the segments (Z1-1 to Z1-14) will evolve depending on the bubble diameter. The representative example of the bubble diameter variation along the VD processing in the respective segments is shown in Fig. 6b. The derivation of the bubble diameter (d_B) is discussed in the following section.

The bubble size distribution in the plume is affected by the flow condition in the respective

Figure 4

Schema representing the plume area (A_p) and the ladle eye area (A_e) (a) and evolution of the dimensionless eye (A_e/A_p) with argon flowrate (b).

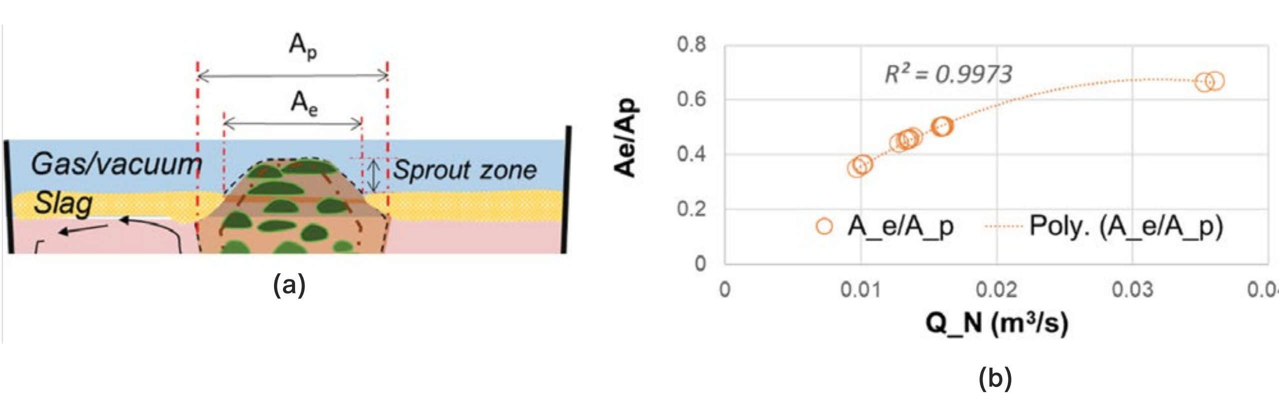

Figure 5

The ladle eye area (A_e): diameters D1 and D2 as obtained from the on-line video monitoring system (a) and evolution of the ladle eye diameter as a function of processing time along with water modeling results (b).[13,14]

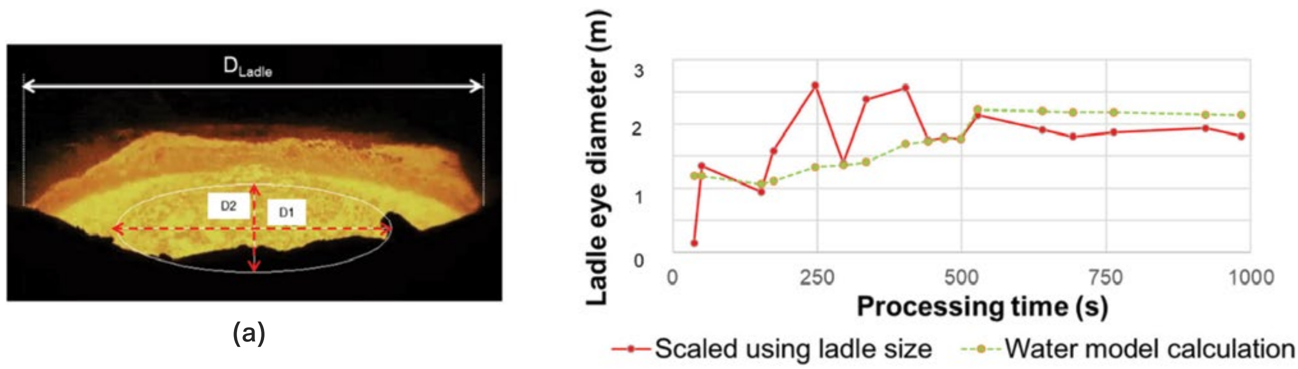

(a) (b)

Figure 6

Schematic representation of implementation of EERZ concept to model gas bubble/steel reaction along with the concentration profile of nitrogen inside the bubble, at Z1 and Z2 (a) and evolution of bubble diameter along the height of the plume (Ar plug to ladle eye) (b).

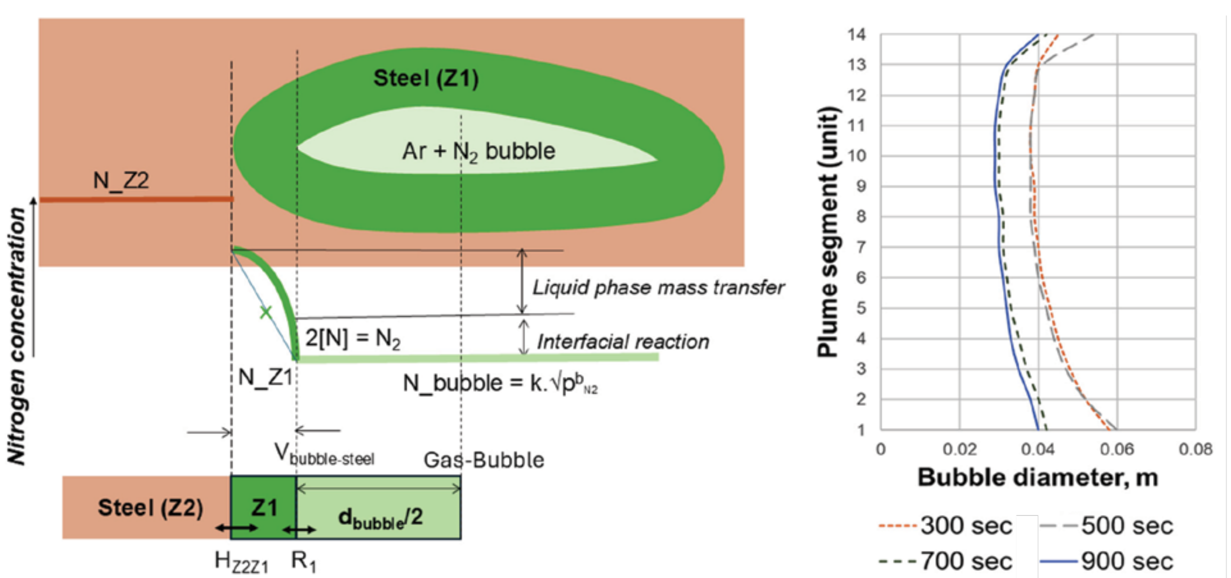

(a) (b)

volume of the plume (Z1-1, Z1_2…Z1_n), bubble coalescence (due to collision) and breakup. The evolution of bubble sizes has been observed in several water modeling experiments.[15–17] From these water modeling experiments, it has been concluded that bubble breakup results from two opposing forces in the liquid steel: (a) turbulence, which promotes bubble distortion, and (b) surface tension, which restores the bubble shape. The frequency of bubble breakup (f_B) can then be attributed to the velocity of the force imbalance per the bubble perimeter (which is proportional to the bubble diameter).[18]

$$f_B = 0.25\frac{\sqrt{8.2\left(\varepsilon d_B\right)^{2/3} - 12\sigma/\left(\rho_L d_B\right)}}{d_B}$$

(Eq. 8)

where ε refers to the energy dissipation rate per unit mass of liquid steel, and σ and ρ_L refers to the surface tension and density of the liquid steel, respectively. In this study the minimum diameter of the bubble (dmin) is calculated by $f_B = 0$. Similarly, coalescence frequency is given as:

$$f_C = 5.77\alpha^2\varepsilon^{1/3}d_B^{-11/3}\exp\left(-1.29\varepsilon^{1/3}d_B^{5/6}\sqrt{\rho_L/\sigma}\right)$$

(Eq. 9)

where α is the volume fraction of bubbles. In Eq. 9 the pre-exponential term represents the collision frequency, and the exponential term dictates the probability of coalescence. Both α and ε (fluid flow energy dissipation) will depend on Ar flowrate and the height in the plume (related actual pressure) during the degassing process and respective plume calculations:

$$\alpha = 0.74\dot{Q}_l^{0.5}\overline{x}^{-1.25}\left(1-\xi\right)^{-1}$$

(Eq. 10)

$$\varepsilon = \frac{\dot{n}_g RT}{\rho_l V_{p,total}}\ln\frac{H+h_a}{h_a}$$

(Eq. 11)

ε will be discussed in the following section on Zone 2 calculations. $\dot{Q}_l$ is the gas flowrate in the steel, which is different than $\dot{Q}_N$ (gas flowrate at standard temperature and pressure). $\dot{n}_g$ is the molar gas flowrate and H and h_a being the liquid steel melt height and height at a given depth. A Microsoft Excel-based bubble diameter calculator was developed which dynamically calculates the α, ε, f_B, f_C and d_B, where ρ_L (7,000 kg/m^3) and σ (1.8 N/m) are kept constant. The bubble diameter (d_B) is calculated by equating f_B and f_C, f_C can vary depending on the α and ε depending on the position inside the plume. The range of calculated in this work 0.03–0.06 m is comparable to that reported by Tang and Pistorius[19] and Bannenberg et al.[4] As shown in Fig. 6b, in this study the evolution of the bubble diameter along the height of the plume is initially large (near the porous plug), decreases subsequently in the mid-height of the ladle (within the plume region), and then increases near the ladle eye. This trend is dissimilar to that discussed by Tang and Pistorius.[19] As the Z1 volume is regarded as an envelope around the bubble, the thickness of this envelope is considered to be a percentage (or fraction) of the bubble diameter. As discussed in a later section, this percentage was a modeling variable and was optimized to reproduce the observed deN in the heats.

c. Zone 2 (Z2): The steel volume inside the plume region is calculated based on Ebneth and Pluschkell's expressions,[20] which are incorporated to develop the Microsoft Excel-based Plume volume solver. The discussion and derivation of the expressions behind the solver were obtained from the references.[19,20]

Fig. 7 shows the schematic of the plume with the Z_n (1-14)-segments and the plume volume/

Figure 7

Schematic diagram of Z2 with 14 Z1 segments (a). Variation of plume radius along the height of the plume at 1 mbar (b) and 1 atm (c) along with data from reference Tang and Pistorius.[19]

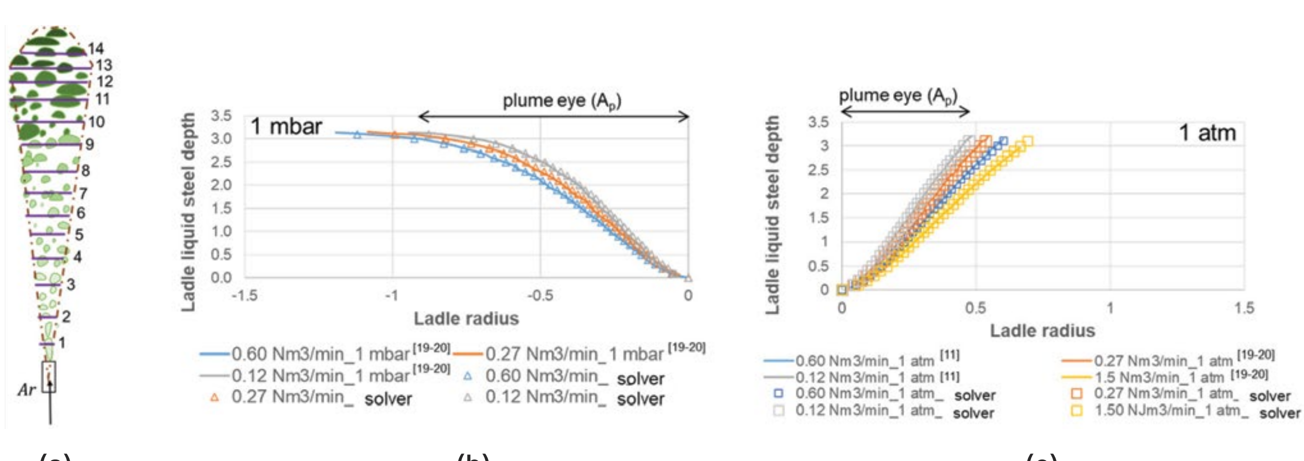

shape as a function of Ar gas flowrate as calculated by the Plume volume solver and presented by Ebneth and Pluschkell[20] for 1 mbar (Fig. 7b) and 1 atm (Fig. 7c) atmospheric pressure.

It should be noted that the plume size at the top part of the ladle, which is close to the ambient atmosphere, varies significantly with the vacuum condition. Such variations significantly influence the ladle open eye size as shown in Fig. 7b and 7c. The expansion in the plume volume under vacuum conditions increases the surface nitrogen desorption from larger bubble surface area (Z_eye) and leads to maximum denitrogenation. For the present EERZ-based VTD model, the Z2 or plume volume is calculated by the process data of Ar gas flowrate and the pressure evolution along the VD processing time, utilizing the Plume volume solver. The VTD model allows spontaneous N2 formation in Z2 (Fig. 3: mode 4).

d. Zone 3 (Z3): Steel outside the plume can be considered relatively stagnant, forming Z3 in the current modeling. Z3 is essentially the difference between the total steel volume and the volumes of Zone 2 and 1. Like Z2, the VTD model allows spontaneous N2 formation in Z3 (Fig. 3: mode 4). Although slag properties have been considered to determine the Z_eye in this EERZ modeling work, steel-slag reactions will not be discussed.

EERZ Modeling Parameters, Tools and Databases

The EERZ modeling primarily relied on the following inputs for respective heats:

a. Chemistry information:
   - i. Steel: Fe-C-Mn-Si-Al-N-O-S.
   - ii. Slag: CaO-Al_2O_3-SiO_2-MgO-MnO-FeO slag phase.

b. Mass information:
   - i. Slag: 1–2 tons.
   - ii. Steel: 135 tons.

c. Temperature: 1,600°C (isothermal condition).

d. Process conditions:
   - i. Pressure of the ambient atmosphere.
   - ii. Argon gas flowrate.

e. Solvers to determine ERZ volumes:
   - i. Plume eye solver.
   - ii. Bubble diameter calculator.
   - iii. Plume volume solver.

f. Thermochemical modeling: FactSage version 8.3[12] was used, with the following databases: FtMisc (for steel), Ftoxid (slag) and FactPS (gas).

The identification of the modeling parameters, tools and databases was succeeded by development of the modeling flow sheet that determined the time variable to predict reaction rates.

VTD Modeling Flow Sheet

A simplified version of the process flow sheet is presented in Fig. 8.

a. at t = 0:
   - i. The steel stream was initialized with the respective composition and temperature entering VTD station. The slag composition, used to calculate Z_eye, is taken into account.
   - ii. The process data for the heat, namely the argon injection and vessel pressure variation profiles and the VD process duration served as input data.

b. at t = 1:
   - i. Based on the input data the respective zones Z_eye, Z1, Z2 and Z3 were calculated.
   - ii. Z_eye area was calculated with the Plume eye solver. The Z_eye thickness was modeled and kept the same as Z1_14 (Z1 section closest to the ladle eye region). Finally, the Z_eye steel mass was reacted with the ambient atmosphere using FactSage-Equilib module according to Fig. 3: mode 3.
   - iii. Z1 steel:
     - i. Volume varied along the segments, determined by the bubble diameter calculator along the plume height.
     - ii. Individual segment (1-14) masses for Z1 (Z1_1 to Z1_14) were considered for deN reactions with the bubbles, as shown in Fig. 3: mode 1-2.
     - iii. Mixing between the steel was considered for adjacent Z1 segments and the steel in Z1 and gas in Z1 bubble was updated.
     - iv. The steel along the different Z1 segments, had different N content, which was governed by the equilibrium deN reaction calculated by the FactSage-Equilib module.
     - v. Gas evolved at Z1 segment 14 was exited the system. The gas evolved from their respective segments were also recorded from the equilibrium FactSage calculations and placed into an Excel file.
   - iv. Z2 steel:
     - i. Volume varied with the Ar gas injection. Z2 was calculated by Plume volume solver.
     - ii. Spontaneous N2 formation in Z2 was allowed (Fig. 3: mode 4).

iii. Z2 was allowed to mix with Z_eye and Z1 steel after a "modeled" homogenization frequency which is denoted at te12N.

v. Z3 steel:

i. Mixed with Z_eye, Z1 and Z2 steel after a "modeled" homogenization frequency, which is denoted at te123N.

ii. Spontaneous N_2 formation in Z3 was allowed (Fig. 3: mode 4).

vi. All the mixing and stream assignment was performed in FactSage-Equilib module with Macro-coding functionality.

c. This iteration was continued for the number of time steps (t_N), which was modeled to be 60 seconds ($t^{e123}{}_N$) in the present work.

The main modeling parameters adjusted to enable the EERZ model to provide accurate predictions of the final N content are as follows:

a. Z_eye thickness was modified from 0.1 m to thickness of the steel/bubble at Z1.

b. Z1 volume was estimated based on the bubble diameter predictions.

c. Homogenization frequencies between Zone 1 and 2 ($t^{e12}{}_N$) and Zone 1, 2 and 3 ($t^{e123}{}_N$).

Fig. 9 shows the iterative nature of Z1 thickness (volume of steel/bubble interface) modeling during the current modeling using the EERZ approach, where Z1 is an envelope of steel and its width was varied from 4%, 12% and 20% of the gas bubble diameter (D_b) in the plume region. As seen in Fig. 9, 12% D_b gave the best fit, where 4% and 20% overpredicted and underpredicted the final N content, respectively. Higher volume of Z1 (20% D_b) will intuitively lead to a sharper drop in N content of the steel.

Results and Discussion

Modeling Results and Discussion: Nitrogen Predictions (Three Heats)

The fixed set of modeling parameters was then applied to simulate the deN process of Heats 1–3. A comparison of the measured and EERZ-model simulated nitrogen contents is presented in Fig. 10. The EERZ model slightly overcalculated the final nitrogen content for Heat 1 (74 ppm vs. measured 70 ppm) and provided precise estimations for Heats 2 (64 ppm) and 3 (53 ppm).

The overestimation of final nitrogen for Heat 1 (~6% error) although minimal can be attributed to zone-specific deN mechanisms and assumptions of the EERZ model. As previously detailed, the removal of nitrogen from steel involves both the reaction of gas bubbles with

Figure 8

The calculation flow sheet for the current VTD model.

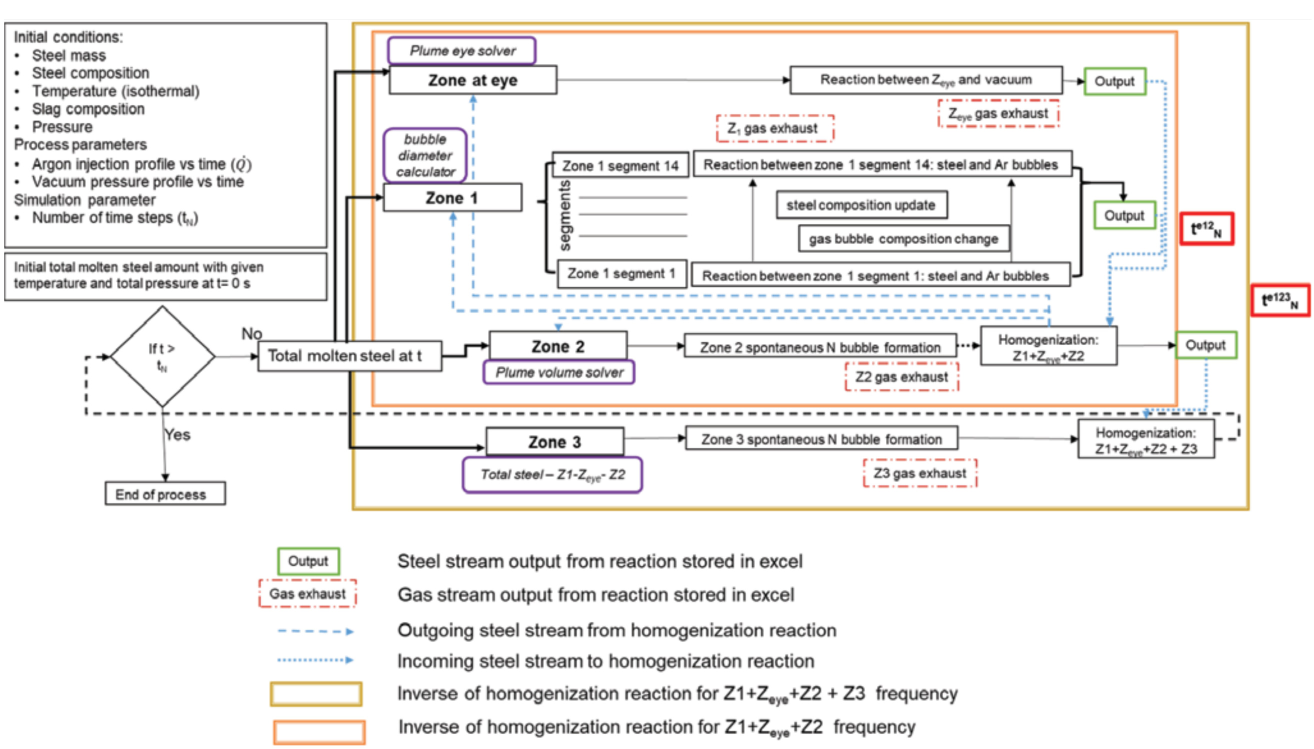

Figure 9

Evolution of nitrogen as a function of Z1 volume estimates based on fraction of gas bubble diameter (D_b) in the plume region.

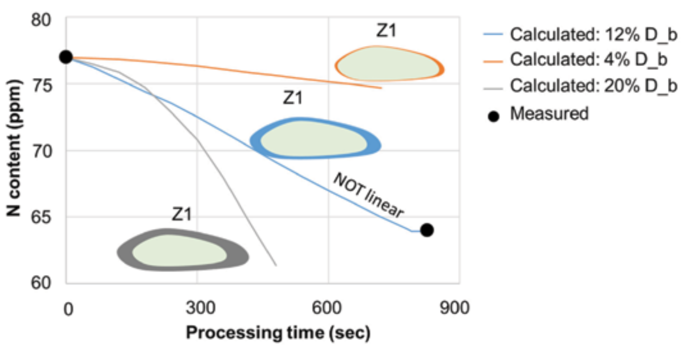

Figure 10

Comparison between the modeled and measured N content for three heats.

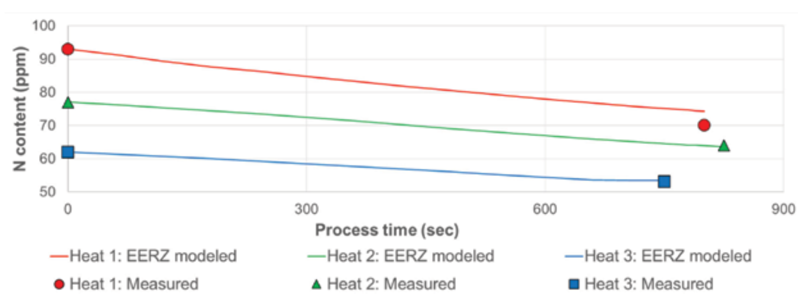

the steel in the plume (Z1) and the interaction of vacuum with the steel exposed at the ladle eye (Z_eye). Both mechanisms have been incorporated into the EERZ model, allowing for the quantification, comparison, and correlation of their contributions to deN relative to the operational conditions of Heat 1's VD operations, such as modifications in Ar flowrate and vacuum conditions.

Fig. 11 illustrates the impact of these two mechanisms in relation to VD operational conditions and the respective masses of Z1 and Z_eye. In Fig. 11a, the y-axis provides an estimate of the nitrogen mass in the offgas from the two sources during Heat 1's degassing. It reveals that the contribution of deN from Z_eye is minimal until the vessel pressure drops to ~<10 torr, as depicted in Fig. 11b, and gradually increases from ~7% to 22% with the onset of deep vacuum conditions. Therefore, in the later stages of degassing, out of the 2,563 g of nitrogen removed from the steel (~135 tons), almost 560 g was removed through the direct reaction of steel and vacuum at the ladle open eye. In Fig. 11a, the N removal rate exhibits a drastic decrease at ~150 second from 4.3 g/second to 2.1 g/second, primarily due to the drop in N removal by Z1 (steel-bubble reaction). This drop can be attributed to the decrease in the steel/bubble interaction volume (Z1 mass fraction), as shown in Fig. 11c, caused

Figure 11

Contribution of Z1 and Z_eye to the nitrogen removed during the complete processing time. The de-N rate (slope) has been superimposed (a). Variation of process parameter (b) and Z1 and Z_eye mass fractions with processing time (c).

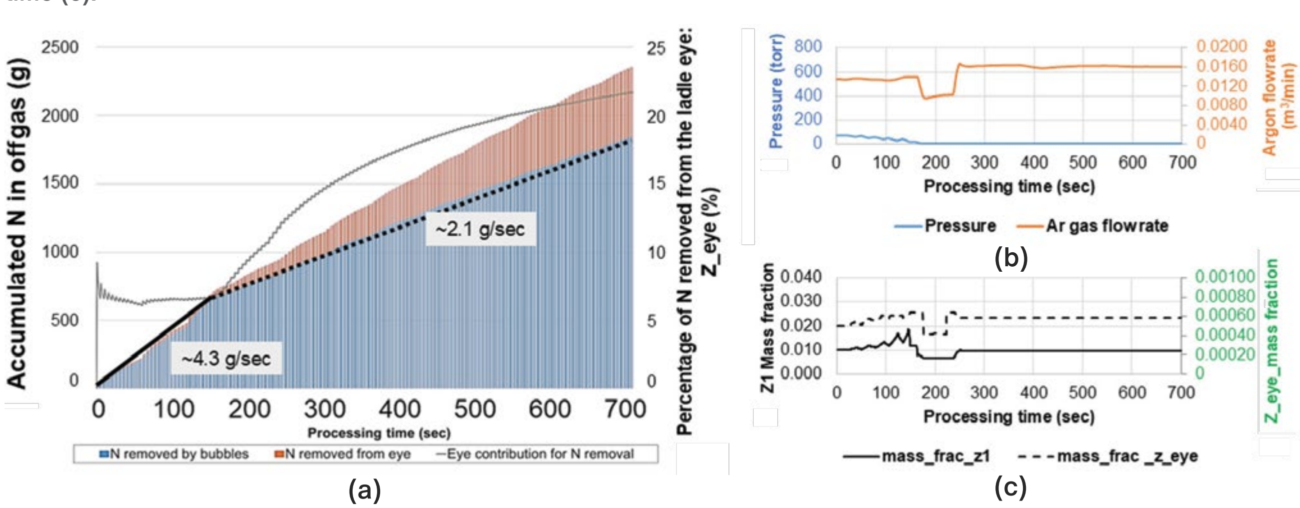

Figure 12

Evolution of the mass fraction of Z1 (steel/bubble interaction) at the top (14), middle (7) and bottom segment (1). (a)–(c) show the evolution of Z1 size and exhaustion of steel due to bubble growth.

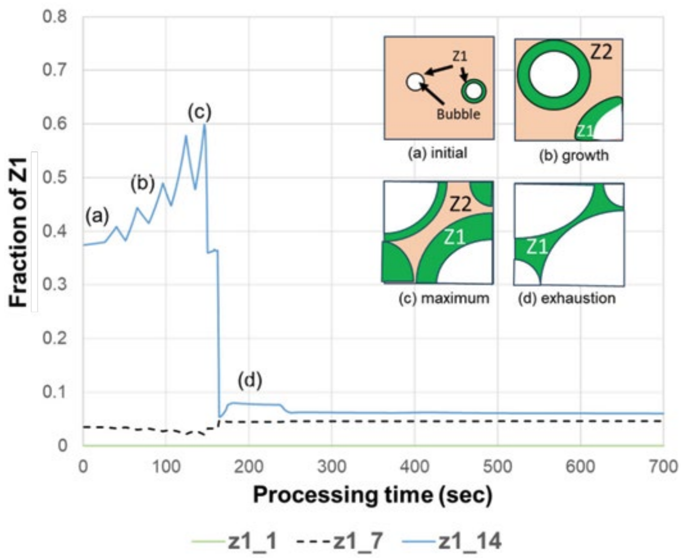

by bubble size reduction during the onset of deep vacuum conditions.

The current EERZ model also indicates that the most intense deN from steel/bubble interaction (Z1 mass) occurs near the surface of the ladle eye, which can be tracked by plotting the Z1 fraction of section 14, 7 and 1. The deN process during the steel/bubble depends on the interaction volume of interacting steel surrounding the bubble: Z1. In Fig. 12, a noticeable drop in the volume of steel/bubble interaction is observed around 150 seconds, as illustrated by the green regions in subfigures (a) to (d).

Also as shown in Fig. 12a–12c, Z1, which has a thickness proportional to the average diameter of the bubbles, experiences an increase in volume as the pressure or Ar gas flow decreases. Under conditions that promote further bubble growth, the formation of closely packed bubbles reduces the volume of steel between them (Z2) which serves as a nitrogen reservoir. This exhaustion of steel volume between bubbles, as illustrated in Fig. 12d, hinders reaction kinetics and retards deN. Consequently, this decrease in steel volume leads to a reduction in the deN rate, as shown in Fig. 11. A similar phenomenon was reported in a study on MnO reduction by CO bubbles.[21] If this hypothesis holds true, it suggests the presence of an optimal range of Ar gas flowrates — sufficient to generate bubbles with an optimal size distribution for effective reaction with the steel, but not so high as to deplete the mass of steel between the bubbles, thereby reducing the N removal rate. While a high vacuum is likely still desirable, as it determines the final equilibrium N content.

Contribution of the EERZs to Denitrogenation in the VTD Model

Fig. 13 illustrates the typical evolution of the four ERZs considered in the current VTD model alongside the change in nitrogen content (-ΔN content) in ppm. The ΔN content was determined by calculating the difference in average N content of the steel bath every 60 seconds of processing time through a homogenization reaction between the zones (Z_eye, Z1, Z2 and Z3). In Fig. 13b, the mass fraction of Z1 gradually doubles, while that of Z_eye, Z2 and Z3 in Figs. 13a, 13c and 13d marginally changed during the VD time. The evolution of Z1 (steel/bubble interaction volume) for the current heat is evident.

Similar correlations between -ΔN content and average Z1 fraction (every 60 seconds of processing time)

Figure 13

A typical evolution of change in the nitrogen content with the mass fraction of Z_eye (a), Z1 (b), Z2 (c) and Z3 (d) as a function of processing time.

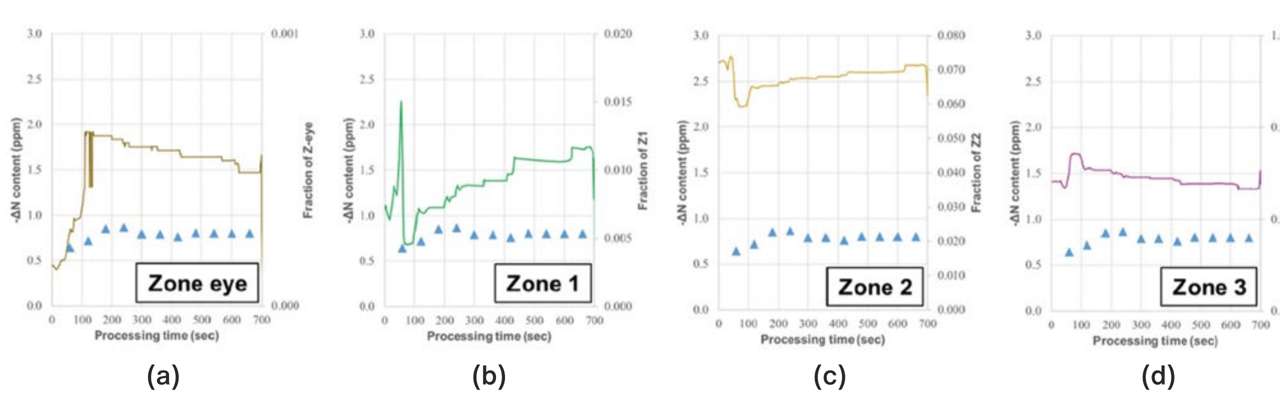

Figure 14

Evolution of average change in the nitrogen content and average Z1 mass fraction for Heat 1 (a), Heat 2 (b) and Heat 3 (c) as a function of processing time.

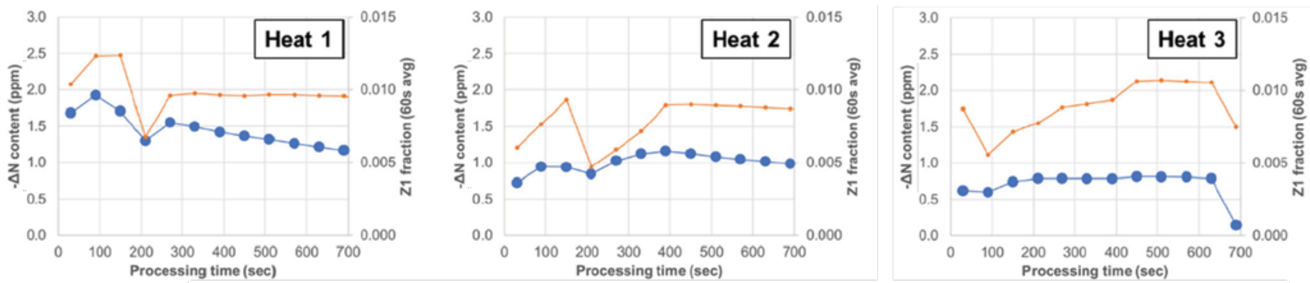

(a) (b) (c)

was observed for all the three heats, which are plotted in Fig. 14.

While the VTD model based on EERZ approach can closely predict the actual N content (as shown in Fig. 10), the calculation of a typical 13-minute degassing process required approximately 24 hours (i7-8 core processor with 16 GB RAM). Consequently, there arose a need for a potential parametric correlation between the operational parameters determining Z1 and the deN rate to facilitate quicker/on-line prediction of the N content.

Simplification of the Model: ΔN Content vs. Average Z1 Correlation

Fig. 15 illustrates the -ΔN content vs. average Z1 fraction for all three heats modeled based on the EERZ approach. In Fig. 15a, a positive correlation is evident between the change in nitrogen content (-ΔN content) and average Z1 fraction. The disparity in the slopes of the regression lines suggests differences in the deN rates among the three heats shown in Fig. 15a. These differences can be ascribed to variations in the driving force within the three heats, which, at any given time, is influenced by the difference between real-time and equilibrium N content. Anticipating minimal equilibrium N content due to the low pressure within the VTD, the driving force (directly proportional to the deN rate) predominantly depends on real-time N content. The validation of this assumption is depicted in Fig. 15b, where the slope of the regression lines in Fig. 15a (representing apparent average removal

Figure 15

Dependency of change in nitrogen content per 60 seconds on the average Z1 volume (a) and correlations between deN rate per unit average Z1 volume and the initial N content (b).

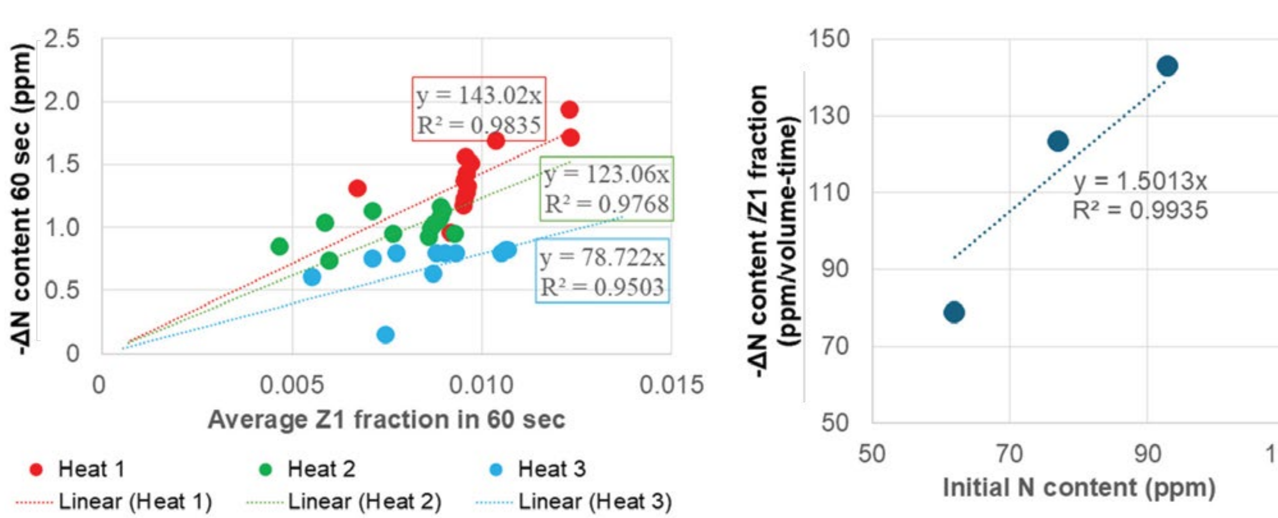

(a) (b)

rates) shows a positive correlation with the initial N content (real-time N content).

For steel grades of similar chemistries, a correlation between the ΔN content and Z1 has been established and extended to include the argon injection pattern (argon flow profile) and vacuum condition. The utilization of the parametric equation, instead of the EERZ-base VTD model, has significantly reduced prediction time and facilitated exploration into avenues for improved VTD process efficiency and control. However, the EERZ-based model remains essential with changes in steel chemistries or process parameters such as temperature, slag depth/chemistry, etc.

Validation of the ΔN Content vs. Average Z1 Correlation and Impact of Surface-Active Elements

The parametric equation has been applied to 22 heats from 12 different steel grades. In Fig. 16a, a comparison between the modeled and measured $[N]_{final}$ is presented, with the red dashed line representing an equivalent correlation and the green dashed line indicating deviation at a lower [N] ppm region. Generally, the predicted and modeled $[N]_{final}$ agree; however, below ~60 ppm, the empirical correlation tends to overpredict $[N]_{final}$. This deviation can be attributed to differences in Z1 (bubble/steel interface) volumes across different steel grades with varying aim chemistries. Previous studies[22,23] have also demonstrated that the deN rate is significantly influenced by active sites (for absorption and desorption) for N at Z1, which are limited by the presence of surface-active elements such as S. The empirical model was developed using steel with a total sulfur (TS) after VTD in the range of 90–120 ppm.

For steel grades with lower TS, more active sites become available at the interface for the transport of nitrogen (N) from the bubble to the steel. This characteristic led the empirical model to underpredict the deN rate and overpredict the final nitrogen concentration: $[N]_{final}$. The difference between the modeled and measured $[N]_{final}$, was plotted against the total sulfur (TS) contents measured for the 22 heats, as shown in Fig. 16b. The decreasing trend suggests that the empirical model will overpredict deN for lower sulfur content, and the best agreement between the model and measured $[N]_{final}$ occurs at TS = 100 ppm, which was the median value of the three heats originally used to develop the EERZ model-based correlation.

Based on this observation, the empirical correlation was corrected, leading to a significant improvement in predictions, especially for low-nitrogen heats, where 17 out of 22 heats had an error of ±7 ppm, and 21 out of 22 heats had an error of ±10 ppm. It should be noted that, although the steel chemistries (see Table 1) vary in C, Mn, and Si, their impact on Z1 were not investigated for further refinement of the empirical correlations.

Discussion and Future Work

In the EERZ model, Zone 3 (Z3), designed as the nitrogen reserve, is presently oversimplified and lacks consideration for the concentration gradient within Z3 arising from variations in mass transfer coefficients. A potential improvement involves refining Z3 through segmentation based on velocity or momentum, although

Figure 16

Comparison of measured and calculated N content (a) and correlation between VTD S level and the difference between modeled and measured N content (b).

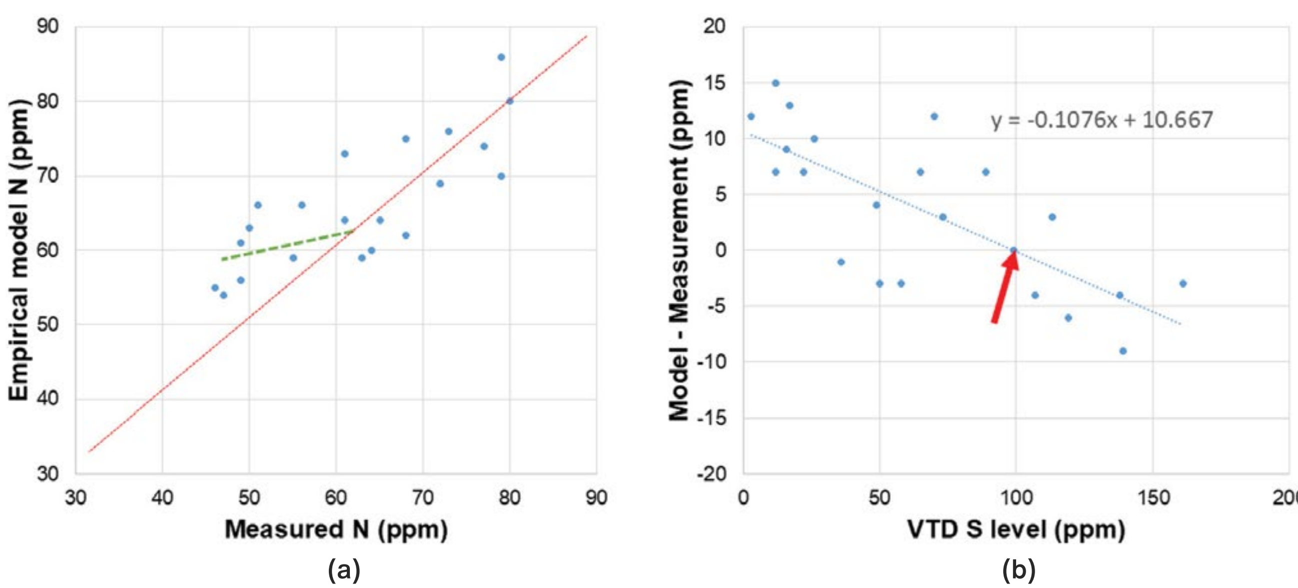

such enhancement may entail an increase in simulation runtime.

Currently, the evaluation of degassing effects on the plume is based on the argon injection rate and pressure, enabling the calculation of bubble and plume sizes. However, as the deN progresses, the gas phase within the bubble increases, likely causing the bubbles to expand. Given that the zone's volume is dictated by interfacial area, current estimations of Z1 and Z2 may be underestimated. Both aspects stand to benefit from the implementation of computational fluid dynamics (CFD) simulations of bubble-induced steel flow in the plume region.

Regarding slag/steel interactions, intense stirring can break the slag and introduce droplets into the liquid steel. Although the current EERZ model will be updated for desulfurization prediction, capturing the effects of slag droplets and the top slag-bubble interactions will require a better understanding of high-temperature slag-gas interactions, which are rarely reported in the literature. Utilizing enhanced image acquisition from actual operations, coupled with advanced image processing, may help bridge this knowledge gap. Incorporating nonisothermal EERZ simulations will also be necessary when subsequent ladle operations such as arcing and alloying are considered.

Conclusions

In the present study, the primary VD operational parameters were reviewed and a kinetic process model of a VTD was established using the EERZ approach.

The VTD model presented here has been simplified to focus on the deN of steel considering three primary reaction zones. The plume region of the VTD has been further subdivided into 14 layers to track the variation of pressure and growth of the Ar gas bubbles. The flexibility provided by EERZ approach has helped the model to simulate the steel/bubble reactions which is the dominant mechanism of deN of steel.

The VTD model was established using process parameters and the ladle open eye data recorded during the VD of three heats. The VTD model was then validated with the endpoint (before and after) steel chemistry VD. The slag compositions were also integrated into to generate the ladle eye calculations.

Correlation was derived between the deN content and the mass of the steel/bubble reaction zone (Z1). The correlation reduced the deN prediction time significantly: 24 hours for EERZ to <1 minute for the correlation. This thermodynamic validity of the correlation was established from its dependence on the initial N content of the heat: which dictates the driving force for deN.

The correlation showed the impact of presence of surface-active elements like sulfur in the steel and the original deN content vs. Z1 fraction was corrected by considering the ladle S.

An EERZ-based model for vacuum tank degassing primarily captures the thermokinetic aspects and complexities of multiphase interactions. Combining these models with additional plant data and CFD simulations will further enhance and refine such simulations. Such comprehensive simulations play a crucial role in process optimization and forecasting maintenance-related delays in steelmaking operations.

Acknowledgments

The authors would like to acknowledge technical input from A. Hamilton and M. Richards (EVRAZ North America R&D) and trial support from R. Zeien (EVRAZ Rocky Mountain Steel). Additionally, the support from the degasser station team of EVRAZ Rocky Mountain Steel is appreciated.

References

1. S. Yu, J. Miettinen and S. Louhenkilpi, "Modeling Study of Nitrogen Removal From the Vacuum Tank Degasser," *Steel Research International,* Vol. 85, No. 9, 2014, pp. 1393–1402.
2. S. Yu, J. Miettinen and S. Louhenkilpi, "Mathematical Modeling of Nitrogen Removal From the Vacuum Tank Degasser," *Steel Research International,* Vol. 86, No. 5, 2015, pp. 467–477.
3. A. Thoms, S. Tu and D. Janke, "Denitrogenation of Steel Melts With Oxygen and Sulphur by Injection of Argon Under Reduced Pressure," *Steel Research,* Vol. 68, No. 11, 1997, pp. 475–478.
4. N. Bannenberg, B. Bergmann and H. Gaye, "Combined Decrease of Sulphur, Nitrogen, Hydrogen and Total Oxygen in Only One Secondary Steelmaking Operation," *Steel Research,* Vol. 63, 1192, 1992, pp. 431–437.
5. S. He, G. Zhang and Q. Wang "Desulfurization Process in RH Degasser for Soft-Killed Ultra-Low-Carbon Electrical Steels," *ISIJ International,* Vol. 52, No. 6, 2012, pp. 977–983.
6. M. Li, Y. Yang, L. Shao and Z. Zhou, "A Numerical Study on Dehydrogenation of Liquid Steel Supersaturated With Hydrogen in a Vacuum Degasser (VD)," *Metall. Mater. Trans. B,* Vol. 54, 2023, pp. 681–693.
7. R. Lichterbeck, J. Laraudogoitia, B. Kleimt, S. Köhle, J. Stender-Robertz and F. Ors, "Dynamic Modelling and Control of the Vacuum Degassing Process: Secondary Steelmaking: Final Report," European Commission, Directorate-General for Research and Innovation, Publications Office, 2001.
8. M. Charlotte, "Influence of Stirring on the Inclusion Characteristics During Vacuum Degassing in a Ladle," master's thesis, KTH, 2015.
9. K. Malmberg and M. Nzotta, A. Karasev and P.G. Jonsson, "Optimization of Stirring Conditions During Vacuum Degassing in Order to Lower Inclusion Content in Tool Steel," *Ironmaking and Steelmaking,* Vol. 40, No. 3, 2013, pp. 231–237.

10. I-H. Jung and M-A. Van Ende, "Computational Thermodynamic Calculations: FactSage From CALPHAD Thermodynamic Database to Virtual Process Simulation," *Metall. Mater. Trans. B,* Vol. 51, 2020, pp. 1851–1874.
11. M-A. Van Ende and I-H. Jung, "A Kinetic Ladle Furnace Process Simulation Model: Effective Equilibrium Reaction Zone Model Using FactSage Macro Processing," *Metall. Mater. Trans. B,* Vol. 48, 2017, pp. 28–36.
12. C.W. Bale, E. Bélisle, P. Chartrand, S.A. Decterov, G. Eriksson, A.E. Gheribi, K. Hack, I-H. Jung, Y-B. Kang, J. Melançon, A.D. Pelton, S. Petersen, C. Robelin, J. Sangster, P. Spencer and M-A. Van Ende, "FactSage Thermochemical Software and Databases, 2010–2016," *Calphad,* Vol. 54, 2016, pp. 33–53.
13. K. Krishnapisharody and G. Irons, "A Model for Slag Eyes in Steel Refining Ladles Covered With Thick Slag," *Metall. Mater. Trans. B,* Vol. 46, 2015, pp. 191–98.
14. K. Krishnapisharody and G. Irons, "Modeling of Slag Eye Formation Over a Metal Bath due to Gas Bubbling" *Metall. Mater. Trans. B,* Vol. 37, 2006, pp. 763–772.
15. M. Zhou and J.K. Brimacombe, "Critical Fluid Flow Phenomenon in a Gas-Stirred Ladle," *Metall. Mater. Trans. B,* Vol. 25, 1994, pp. 681–693.
16. P.E. Anagbo and J.K. Brimacombe, "Plume Characteristics and Liquid Circulation in Gas Injection Through a Porous Plug," *Metall. Mater. Trans. B,* Vol. 21, 1990, pp. 637–648.
17. A. Alexiadis, P. Gardin and J.F. Domgin, "Spot Turbulence, Breakup, and Coalescence of Bubbles Released From a Porous Plug Injector Into a Gas-Stirred Ladle," *Metall. Mater. Trans. B,* Vol. 352004, pp. 949–56.
18. P.C. Pistorius, *Bubbles in Process Metallurgy,* Vol. 2, Elsevier Ltd., 2013.
19. D. Tang and P.C. Pistorius, "Kinetics of Nitrogen Removal From Liquid Third Generation Advanced High-Strength Steel by Tank Degassing," *Metall. Mater. Trans. B,* Vol. 53, pp. 2022, 1383–1395.
20. G. Ebneth and W. Pluschkell, "Dimensional Analysis of the Vertical Heterogeneous Buoyant Plume," *Steel Res.,* Vol. 56, 1985, pp. 513–518.
21. B.J. Jamieson, Y. Tabatabaei, M. Barati and K.S. Coley, *Metall. Mater. Trans. B,* Vol. 50, 2019, pp. 192–203.
22. R.J. Fruehan, D. Goldstein, B. Sarma, S.R. Story, P.C. Glaws and H.U. Pasewicz, "Recent Advances in the Fundamentals of the Kinetics of Steelmaking Reactions," *Metall. Mater. Trans. B,* Vol. 31, 2000, pp. 891–898.
23. R.J. Fruehan and L.J. Martonik, "The Rate of Absorption of Nitrogen Into Liquid Iron Containing Oxygen and Sulfur," *Metall. Mater. Trans. B,* 1980, Vol. 11, pp. 615–621.

This paper was presented at AISTech 2024 — The Iron & Steel Technology Conference and Exposition, Columbus, Ohio, USA, and published in the AISTech 2024 Conference Proceedings.